Sequential evolution of virulence and resistance during clonal spread of community-acquired methicillin-resistant *Staphylococcus aureus*

Richard Copin[a,1], William E. Sause[b,1], Yi Fulmer[a], Divya Balasubramanian[b], Sophie Dyzenhaus[b], Jamil M. Ahmed[a], Krishan Kumar[a], John Lees[b], Anna Stachel[a], Jason C. Fisher[c], Karl Drlica[d,e], Michael Phillips[a], Jeffrey N. Weiser[b], Paul J. Planet[f], Anne-Catrin Uhlemann[g], Deena R. Altman[h,i], Robert Sebra[i], Harm van Bakel[i], Jennifer Lighter[j,2], Victor J. Torres[b,2], and Bo Shopsin[a,b,2]

[a]Division of Infectious Diseases and Immunology, Department of Medicine, New York University School of Medicine, New York, NY 10016; [b]Department of Microbiology, New York University School of Medicine, New York, NY 10016; [c]Division of Pediatric Surgery, Department of Surgery, New York University School of Medicine, New York, NY 10016; [d]Public Health Research Institute, New Jersey Medical School, Rutgers Biomedical and Health Sciences, Rutgers University, Newark, NJ 07103; [e]Department of Microbiology, Biochemistry, and Molecular Genetics, New Jersey Medical School, Rutgers Biomedical and Health Sciences, Rutgers University, Newark, NJ 07103; [f]Department of Pediatric Infectious Disease, Children's Hospital of Philadelphia, Philadelphia, PA 19104; [g]Division of Infectious Diseases, Department of Medicine, Columbia University Medical Center, New York, NY 10032; [h]Division of Infectious Diseases, Department of Medicine, Icahn School of Medicine at Mount Sinai, New York City, NY 10029; [i]Department of Genetics and Genomic Sciences, Icahn School of Medicine at Mount Sinai, New York, NY 10029; and [j]Division of Pediatric Infectious Diseases, Department of Pediatrics, New York University School of Medicine, New York, NY 10016

Edited by Emil C. Gotschlich, The Rockefeller University, New York, NY, and approved December 6, 2018 (received for review August 17, 2018)

The past two decades have witnessed an alarming expansion of staphylococcal disease caused by community-acquired methicillin-resistant *Staphylococcus aureus* (CA-MRSA). The factors underlying the epidemic expansion of CA-MRSA lineages such as USA300, the predominant CA-MRSA clone in the United States, are largely unknown. Previously described virulence and antimicrobial resistance genes that promote the dissemination of CA-MRSA are carried by mobile genetic elements, including phages and plasmids. Here, we used high-resolution genomics and experimental infections to characterize the evolution of a USA300 variant plaguing a patient population at increased risk of infection to understand the mechanisms underlying the emergence of genetic elements that facilitate clonal spread of the pathogen. Genetic analyses provided conclusive evidence that fitness (manifest as emergence of a dominant clone) changed coincidently with the stepwise emergence of (*i*) a unique prophage and mutation of the regulator of the pyrimidine nucleotide biosynthetic operon that promoted abscess formation and colonization, respectively, thereby priming the clone for success; and (*ii*) a unique plasmid that conferred resistance to two topical microbiocides, mupirocin and chlorhexidine, frequently used for decolonization and infection prevention. The resistance plasmid evolved through successive incorporation of DNA elements from non-*S. aureus* spp. into an indigenous cryptic plasmid, suggesting a mechanism for interspecies genetic exchange that promotes antimicrobial resistance. Collectively, the data suggest that clonal spread in a vulnerable population resulted from extensive clinical intervention and intense selection pressure toward a pathogen lifestyle that involved the evolution of consequential mutations and mobile genetic elements.

MRSA | evolution | antimicrobial resistance | virulence

Community-acquired methicillin-resistant *Staphylococcus aureus* (CA-MRSA) strains have dramatically increased the global burden of *S. aureus* infections. CA-MRSA consists of multiple lineages; however, specific geographic regions are usually dominated by a single subclone, with different subclones present in different regions. For example, the pandemic sequence type USA300 is dominant in the United States (1–4). Among the well-known problems caused by USA300 are outbreaks of skin abscesses in high-risk communities (e.g., jails and daycare facilities) (5). Despite considerable research, how epidemic strains of CA-MRSA become established in different settings, especially community settings, is poorly understood.

Although epidemiological risk factors, such as human activities that increase infection risk, are often the primary trigger for clonal spread of pathogens, genome-wide surveys of pathogen populations promise insight into the evolutionary processes and the genetic basis underlying the emergence of successful lineages (6–12). Indeed, genomic comparisons between successful CA-MRSA clones and distantly related strains have provided broad insight into genome evolution within *S. aureus* (13–17). For example, genome-wide studies have described the evolutionary history and spread of successful pandemic clones and have defined the contributions of mutation and recombination to genetic variation in the species (reviewed in ref. 18). They have also pinpointed syndrome-specific elements, such as the prophage-encoded Panton-Valentine

Significance

Epidemics of community-acquired methicillin-resistant *Staphylococcus aureus* (CA-MRSA) are of growing medical concern. To understand the emergence of virulence and antimicrobial resistance, both of which promote CA-MRSA spread, we examined an on-going disease cluster within an enclosed community by analyzing the genome sequences of CA-MRSA clones characterized by high prevalence and a profound persistence. Metabolic adaptation and a phage primed the clone for success, and then a fully optimized variant was created by selection of plasmid-mediated biocide resistance. The data provide mechanistic insight and indicate that high-risk populations are incubators for evolution of consequential phenotypes. Immediate interruption of this evolutionary pattern is essential for forestalling dissemination of resistance from high-risk communities to hospitals and the general population.

Author contributions: R.C., W.E.S., J. Lighter, V.J.T., and B.S. designed research; R.C., W.E.S., Y.F., D.B., S.D., J.M.A., K.K., A.S., J.C.F., M.P., and D.R.A. performed research; R.C., J. Lees, P.J.P., A.-C.U., R.S., and H.v.B. contributed new reagents/analytic tools; R.C., W.E.S., D.B., and S.D. analyzed data; and R.C., W.E.S., K.D., J.N.W., V.J.T., and B.S. wrote the paper.

The authors declare no conflict of interest.

This article is a PNAS Direct Submission.

Data deposition: All genomic data reported in this paper have been deposited in the National Center for Biotechnology Information BioProject database (accession no. PRJNA497094).

[1]R.C. and W.E.S. contributed equally to this work.

[2]To whom correspondence may be addressed. Email: Bo.Shopsin@nyumc.org, Victor.Torres@nyumc.org, or Jennifer.Lighter@nyumc.org.

This article contains supporting information online at www.pnas.org/lookup/suppl/doi:10.1073/pnas.1814265116/-/DCSupplemental.

Published online January 11, 2019.

leukocidin, that are associated with skin and soft tissue infections and that promote transmission (19). Collectively, prior work creates a framework upon which evolution studies can investigate adaptations underpinning the emergence of clones of public health concern within a background of closely related competing strains. Identification of such adaptations is key to finding new therapeutic directions, since the spectrum of adaptive changes that arises during the course of CA-MRSA spread is likely to identify genetic pathways critical for bacterial pathogenesis in vivo.

Human populations having above-average risk of infection (e.g., due to differences in exposure to infection and/or defects in preexisting immunity) are likely important for the initial spread of epidemic CA-MRSA clones. The present report describes a prolonged, ongoing spread of a USA300 clone causing infections in a high-risk community in Brooklyn, New York. Prolonged pathogen circulation represents a unique opportunity for understanding how CA-MRSA adapts to both clinical intervention and to unique aspects of bacterial pathophysiology underlying heightened infection risk. We used whole-genome sequencing of 86 isolates obtained from infected children and adults over a 2-y period, followed by comparative analyses, to reconstruct the evolutionary steps that led to the emergence of an adapted MRSA strain in a previously unrecognized high-risk population. For convenience, we call the adapted strain the USA300-Brooklyn variant (USA300-BKV). We found distinct single-nucleotide polymorphisms (SNPs) and larger structural changes that help explain the success of the USA300-BKV clone. Phenotypic analyses further showed how genetic alterations can affect virulence and antibiotic resistance. The evolution of the USA300-BKV clone supports the hypothesis that human exposures and selection pressures that occur in populations at high risk for infection result in dangerous bacterial adaptation. The study underscores the need for rapid pathogen containment in such situations.

Results

High Prevalence of MRSA Infection Among Pediatric Patients from an Orthodox Jewish Community. Clinical reports of increasing numbers of CA-MRSA infections in our hospital among pediatric Orthodox Jewish children from Brooklyn, New York, led us to investigate the risk of MRSA infection among Orthodox Jewish patients. From May 2015 to December 2016, we identified 4,368 children aged 0 to 18 y who were admitted to our pediatric general and intensive care units (ICUs). Community members were identified on the basis of postal (zip) code, a surrogate for Orthodox-predominant neighborhoods in Brooklyn (20). Medical record review, using clinical criteria plus isolation of *S. aureus* from a normally sterile body site, was used to distinguish infection from colonization. The MRSA infection rate per 1,000 admissions was 10-fold higher among children from Orthodox-associated zip codes than that from other zip codes in New York City (80.2 vs. 8.1, $P < 0.001$) (*SI Appendix*, Table S1). We also determined the prevalence of MRSA colonization upon admission for the general pediatric ward and ICU. Nasal and throat swabs were collected upon admission for 451 patients. Colonization by MRSA was twofold higher in children from high-risk (Orthodox-associated) zip codes as compared to children admitted from all other zip codes, labeled "low-risk" [7% (10/127) vs. 3% (11/324), $P = 0.04$]. No difference was observed in methicillin-susceptible *S. aureus* colonization prevalence or in risk factors predisposing for MRSA acquisition. To our knowledge, correlations between the Orthodox Jewish community and risk of MRSA infection have not been previously described. The clinical characteristics of the subjects studied are described in detail elsewhere. Whether common sources serve as a reservoir for MRSA acquisition and, potentially, the spread of the USA300-BKV clone remains to be determined.

Phylogeny Indicates Spread of a Clone of CA-MRSA Strain USA300 in the Community. We collected consecutive, single-patient isolates of MRSA from infected community members residing in Orthodox-associated zip codes during a 2-y period of medical record review (clinical characteristics and antimicrobial susceptibilities are described in Dataset S1). Ninety-two MRSA isolates from community members were obtained; 84 were from children (42 females) who ranged in age from <1 mo to 18 y, and eight isolates were from adults (four females). The mean age of children in the study was 2.9 ± 3.8 y; 71 patients presented with skin abscesses. Molecular typing results indicated that all isolates were a clone of the epidemic CA-MRSA strain USA300 [*spa* type t008 or a related repeat type, staphylococcal cassette chromosome *mec* type IV (SCC*mec*IV), arginine catabolic mobile genetic element (ACME), and *pvl* positive; these characteristics define USA300 clones (21, 22)] (Dataset S1). Thus, the USA300 clone was associated predominantly with skin infections, consistent with data indicating that the USA300 clone is currently the most frequent cause of purulent skin infection in US emergency departments (2).

To establish whether, and to what extent, infections reflect dissemination of a specific USA300 subclone, we used whole-genome sequencing with mapping of the individual genome sequences against the reference MRSA strain, USA300_FPR3757 (NC_007793.1). Phylogenetic reconstruction was used to compare the 92 community isolates with 16 USA300 control isolates obtained from patients residing in low-risk zip codes (Dataset S1). We observed that 93% (86/92) of isolates from Orthodox community patients (USA300-BKV isolates) clustered within a unique clade, consistent with dissemination of a clone. On average, USA300-BKV isolates differed from one another by 79 SNPs, ranging from 1 to 144 SNPs. None of the control isolates was found within the clade (Fig. 1*A*).

To determine the genomic relationship between USA300-BKV isolates and other USA300 strains in New York City, we compared high-risk genomes with 68 USA300 strains that were collected in a comprehensive community-based study of MRSA transmission in northern Manhattan and the Bronx (Fig. 1*B*) (23, 24). Representatives of all phylogenetic subclades in the parent study were included in the analysis, capturing most of the global diversity of the USA300 lineage. Remarkably, none of these New York City USA300 strains clustered with the USA300-BKV subclade (Fig. 1*B*).

With the same dataset, we used a bayesian approach and the collection dates of each strain as calibration points to estimate the date of origin of the most recent common ancestor of the USA300-BKV cluster (Fig. 1*C*). As in the study of USA300 strains in northern Manhattan mentioned above (24), we predicted the date of divergence of the USA300 epidemic lineage from its most recent common ancestor to be around 1993. We estimated the divergence of the USA300-BKV subclade to have occurred much more recently, around 2005. Additionally, a second branching event within the clade occurred in 2008 (Fig. 1*C*). The nucleotide substitution rate among USA300-BKV isolates was similar to the rate of the broader USA300 lineage (24) (1.41×10^{-6} substitutions per site per year; 95% CI, 7.48×10^{-7}, 2.09×10^{-6}). Thus, mutation rates were not elevated in the USA300-BKV strains.

A Mutation in pyrR Enhances the Fitness of USA300-BKV Clones. Adaptive mutations that may have contributed to the initial success of the USA300-BKV clone should appear in all isolates of the clone but be absent from non-USA300-BKV–associated isolates. USA300-BKV isolates shared 20 unique nonsynonymous SNPs and a stop-gain mutation affecting genes whose products were primarily involved in metabolism of amino acids (*aroD*, *arcB*, *metK*) and carbohydrates (*licR*, *melR*, *glvC*, *setC*, *ddh*, *pyc*) (*SI Appendix*, Table S2 and Dataset S2). Four mutated genes (*licR*, *glvC*, *arcB*, and *fadA*) have been shown to be negatively regulated through carbon catabolite repression (25–28). Carbon catabolite

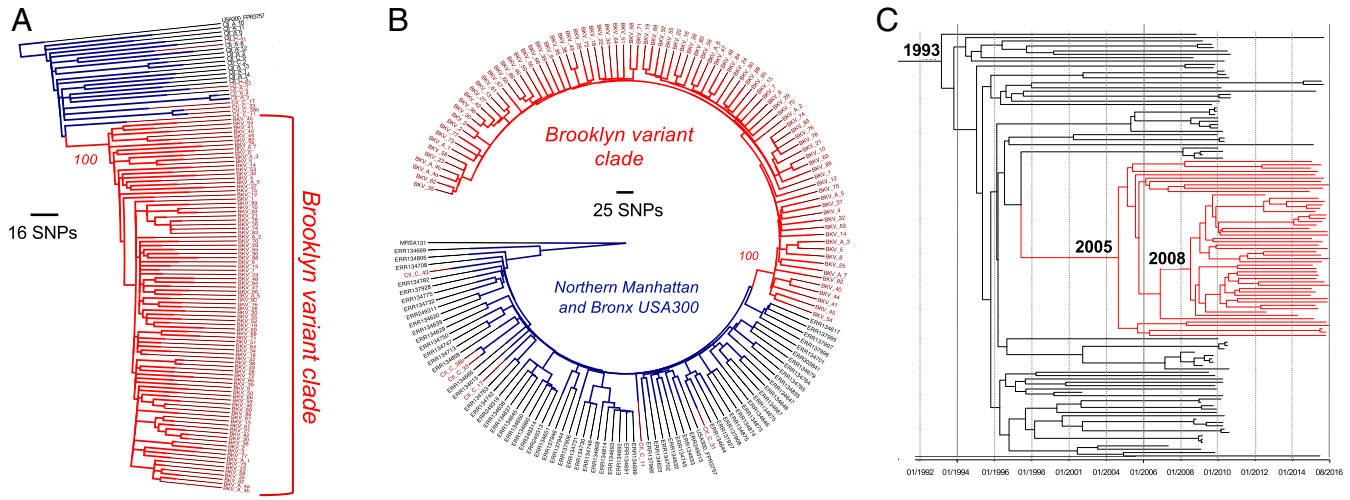

Fig. 1. Bacterial phylogeny reveals the emergence and spread of a dominant clone (USA300-BKV) in the Orthodox Jewish community. Maximum-likelihood phylogenetic trees of 92 isolates obtained from patients residing in Orthodox-associated zip codes (shown in red) compared with (*A*) 16 representative USA300 isolates from adults and children in the same hospital or (*B*) 68 USA300 strains from northern Manhattan and the Bronx. Ninety-three percent (86/92) of isolates from patients residing in Orthodox-associated zip codes clustered within a unique clade (USA300-BKV; BKV clade in red). The remaining six isolates from patients residing in high-risk zip codes clustered with contemporary isolates from our hospital and isolates from northern Manhattan and the Bronx. The trees are rooted using USA300_FPR3757 and the distantly related *S. aureus* isolate MRSA131 as outgroups. Bootstrapping value for the USA300-BKV clade divergence branch is indicated. (*C*) Bayesian phylogenetic reconstruction of BKV isolates estimated from core genome mutations. USA300-BKV clade branches are highlighted in red. Predicted dates of divergence from a most recent common ancestor are indicated.

repression allows bacteria to preferentially utilize rapidly metabolizable carbon sources (e.g., glucose), thereby increasing fitness (29).

Mutation of the regulator of the pyrimidine nucleotide biosynthetic operon (*pyrR*) was particularly interesting. Inactivation of *pyrR*, a transcription repressor that responds to levels of uracil, results in up-regulation of carbamoyl phosphate synthetase (*carAB*). *S. aureus* carries only one form of *carAB*, which is essential for both arginine and pyrimidine biosynthesis (Fig. 2*A*; reviewed in ref. 30). When the sequences of *pyrR* orthologs were aligned, the mutation occurred near conserved residues previously identified by mutagenesis of *Bacillus subtilis* as inactivating *pyrR*, suggesting that the *pyr* mutation was inactivating (31, 32). Accordingly, we tested for functional effects using clinical *pyr* mutant

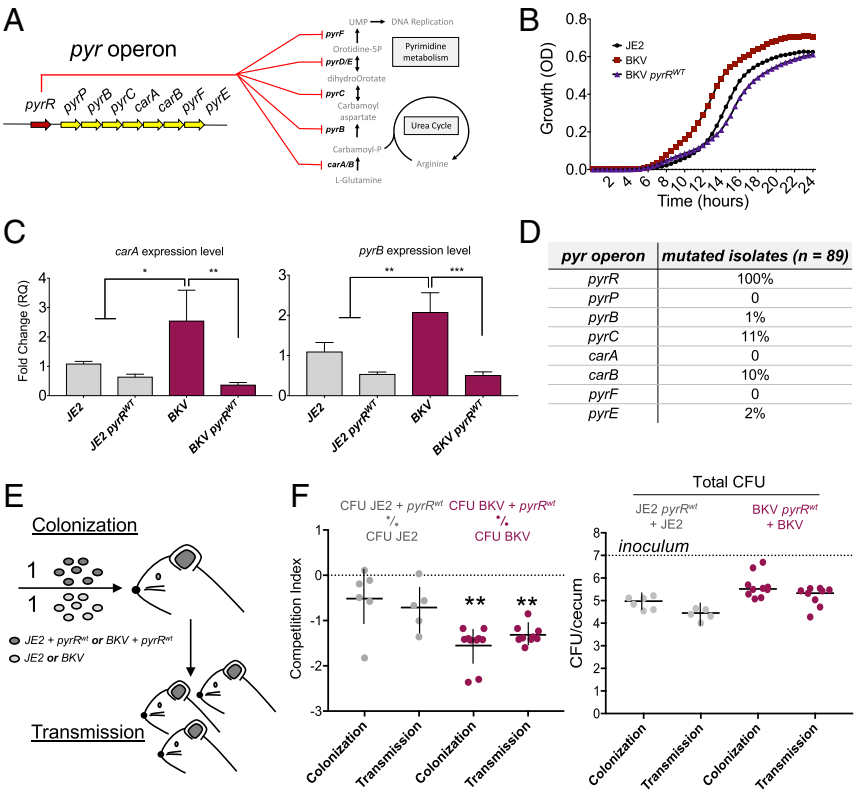

pyr operon	mutated isolates (n = 89)
pyrR	100%
pyrP	0
pyrB	1%
pyrC	11%
carA	0
carB	10%
pyrF	0
pyrE	2%

Fig. 2. A single mutation in *pyrR* affects *S. aureus* fitness in vitro and in vivo. (*A*) Schematic of *pyrR* regulation of *S. aureus* pyrimidine biosynthetic and urea pathways through *pyr* operon gene repression. (*B*) Growth curves of USA300-BKV isolates (BKV isolates) and *pyrR*-complemented BKV isolates in pyrimidine-limited chemically defined medium. (*C*) Real-time qPCR validation of the impact of *pyrR* mutation on *pyr* operon genes *carA* and *pyrB*. Gene expressions were normalized to *pyrR* gene. Data represent mean ± SD (n = 3). $^{*}P < 0.05$, $^{**}P < 0.01$, $^{***}P < 0.001$ using ANOVA with multiple t test comparisons. (*D*) Number of unique mutations targeting *pyr* genes in independent BKV-isolate genomes. (*E*) Schematic of the mouse model of colonization and transmission. Parental mice were orally inoculated with a 1:1 ratio of 10^7 cfu of USA300 strain JE2 + $pyrR^{WT}$ vs. JE2 (a control strain of USA300) or strain USA300-BKV + $pyrR^{WT}$ vs. BKV isolate. Ceca were harvested after 4 d of colonization. (*F*) Competitive colonization and transmission assay (competitive index, *Left*) and quantification of bacteria in stool (cfu, *Right*) were determined from the cecum of inoculated (colonization) and cohoused pups (transmission). Transmission indicates quantification of bacteria in the stool of uninoculated mice that were cohoused with inoculated mice. Median values are shown, and each symbol is the CI from one mouse (*Left*) or cfu from single mouse (*Right*). $^{**}P < 0.01$ by Wilcoxon signed-rank tests.

strains and assayed growth in chemically defined media containing uracil (Fig. 2*B*). For this measurement, we employed a USA300-BKV clinical clone complemented with a chromosomally integrated wild-type (WT) *pyrR*. The *pyrR* mutation enhanced growth of the clinical isolate compared with the complemented clone, suggesting that mutation of *pyrR* increased fitness in energy-poor environments. Moreover, real-time quantitative PCR showed that the *pyrR* mutation enhanced transcription of *pyr* operon genes *carA* and *pyrB* (Fig. 2*C*), indicating inactivation of PyrR-mediated transcription repression.

Two additional observations suggested that the *pyr* mutation was biologically important. First, unique nonsynonymous mutations in other members of the *pyr* operon occurred in independent descendants of clones containing the USA300-BKV–associated *pyrR* mutation (Fig. 2*D*). Independent mutations in the same gene or operon evolving in parallel within individual patients (convergent evolution) suggests compensation for *pyr* operon overexpression through attenuating mutations. Consistent with this hypothesis, we found no evidence of mutation in *pyr* operon alleles among strains from control isolates from our hospital and isolates from northern Manhattan and the Bronx. Compensatory mutations may result from functional trade-offs, wherein inactivating mutations in *pyrR* may enhance fitness in certain vulnerable human populations, while representing a liability to clones in other environments. Second, examination of publicly available genome sequences identified a unique nonsynonymous mutation in *pyrR* as one of the few mutations common to all strains in an independent outbreak of CA-MRSA skin infections among 12 hospitalized children during a 6-mo outbreak in a postnatal ward (33). We found no other *pyr*R mutations in the public database. Collectively, these observations support the hypothesis that skin and soft tissue disease clusters exert selective pressure on *pyr* operon biosynthesis.

Although *pyr* operon-regulated arginine and pyrimidine biosynthesis is known to be critical for virulence in vivo (34–37), the *pyrR* mutation associated with the USA300-BKV clone did not significantly enhance virulence in a murine skin infection model in which lesion size and bacterial cfu were measured (*SI Appendix*, Fig. S1). These observations suggest that the virulence effects of pyrimidine biosynthesis reflect a requirement for a threshold level of expression.

The effects of *pyr* operon-regulated biosynthesis on commensalism are largely unknown. The majority of USA300-BKV infections in children were purulent skin and soft tissue infections [82% (64/78)] that frequently occurred in the groin/buttock area of children aged <1 y, possibly related to skin breakdown from exposure to wet or soiled diapers. At least three observations support the idea that enteric carriage is highly relevant to the spread of CA-MRSA clones. First, it is known that CA-MRSA frequently colonizes the gastrointestinal tract of infants and that broken skin can serve as a nidus for infection (38, 39). Second, in children with CA-MRSA skin infections, the rectum and perianal skin was the key site of colonization (38–41). Third, recent work involving a combination of a murine model of *S. aureus* gastrointestinal colonization and field studies in humans identified interactions between the global virulence regulator *agr* and the gut microbiota as the dominant risk for *S. aureus* carriage (42). To assess the in vivo impact of the *pyrR* mutation, we examined colonization by the USA300-BKV clone in a mouse model of gastrointestinal colonization and transmission (Fig. 2 *E* and *F*). USA300-BKV isolates showed a significant colonization and transmission advantage in the mouse intestine with respect to the same isolates carrying a WT copy of *pyrR* (Fig. 2*F*). Collectively, the data provide experimental evidence for the *S. aureus pyr* operon being a colonization determinant, as previously seen with *Escherichia coli* and *Salmonella* (43, 44). The data also (*i*) indicate that *pyrR* mutation confers an advantage to the bacterium during competition with other strains both in culture and in the mammalian intestine, and (*ii*) suggest that mutation of *pyrR* enhances commensal rather than pathogenic fitness.

A Mosaic Version of Phage ϕ11 in USA300-BKV Isolates Enhances Abscess Formation. We next examined the possibility that mobile genetic elements contributed to the success of the USA300-BKV clone, beginning with an analysis of phage content. The genomes of half (41/86) of the USA300-BKV isolates contained a 42-kb prophage variant of ϕ11 (NC_004615) (Fig. 3*A*). Phage ϕ11 belongs to the integrase group Sa5, members of which integrate into an intergenic region in the *S. aureus* chromosome (45, 46). Sa5 homologs were present infrequently outside the high-risk Orthodox community in New York [16% (62/387)] (24). A mosaic block of 24 genes, which affects the lysogeny and DNA replication modules, contained sequences that are unrelated to ϕ11 or other known prophages; thus, the block might have arisen by a recombination event (Fig. 3 *A* and *B*).

Examination of the distribution of the mosaic prophage among USA300-BKV isolates showed that it clustered with the proximal portions of the phylogeny, indicating that it was a defining feature at an early stage of the lineage evolution and suggesting that, as with the *pyrR* mutation, it may have primed the clone for success (Fig. 3*C*). The absence of the phage from some of the branches of the more distal tips of the phylogeny suggests the ability to reactivate and excise, possibly owing to prophage mobilization during antimicrobial treatment. Indeed, subinhibitory concentrations of antibiotics induce bacteriophage excision and replication (47, 48); moreover, phage excision is frequent among clinical isolates associated with invasive infection (49–52). However, variants that lost the phage often represented a terminal node in phylogenic trees, suggesting that infections are likely selective for the maintenance of mosaic phage.

To determine whether the mosaic phage modulates virulence, we tested for phenotypes in several isolates representative of different phases of USA300-BKV clone evolution based on the phylogeny (Fig. 3*D*). A laboratory strain of USA300-LAC and a USA300 isolate from our hospital not associated with USA300-BKV were used as controls. All naturally occurring isolates from the high-risk Orthodox population demonstrated indistinguishable exoprotein profiles. Core genome-encoded toxins play an important role in CA-MRSA skin infection (53, 54), and cytotoxicity measurements can be used to determine the potential for CA-MRSA strains to cause disease (55). Cytotoxicity assays indicated that cell-free extracts from cultures of the USA300-BKV strain tended to be highly cytotoxic toward primary human neutrophils, irrespective of the presence or absence of the mosaic phage (*SI Appendix*, Fig. S2). Thus, in vitro analyses of cytotoxicity toward human neutrophils do not predict the relative virulence of phage-containing strains.

To determine how well in vitro data translate to the in vivo skin environment, we examined eight representative clinical USA300-BKV strains, five of which encoded the phage, in a murine skin abscess model of infection (56, 57). Each of the strains chosen was similarly cytotoxic in vitro. USA300-BKV strains that contained the mosaic phage formed larger abscesses compared with control strains and USA300-BKV strains that lacked the phage (Fig. 3*D*).

To better understand the contribution of the phage to virulence, we tested for in vivo virulence phenotypes in mosaic phage and WT ϕ11 (NC_004615, from strain RN6734) lysogens derived from strain USA300-LAC. Strikingly, a USA300-LAC strain containing mosaic ϕ11 showed a 50% increase in abscess size over USA300-LAC and USA300-LAC containing the WT ϕ11 (Fig. 4). Testing a higher bacterial inoculum revealed more prominent differences in lesion size, but not in bacterial cfu or dermonecrosis (Fig. 4 and *SI Appendix*, Figs. S3 and S4), perhaps owing to enhanced proinflammatory and/or cytotoxic properties of the USA300-BKV clone. Based on these data, we conclude that (*i*) the effect of mosaic ϕ11 was not due to *cis*-acting effects on genes flanking the phage attachment site (both phages integrated at the same site in the

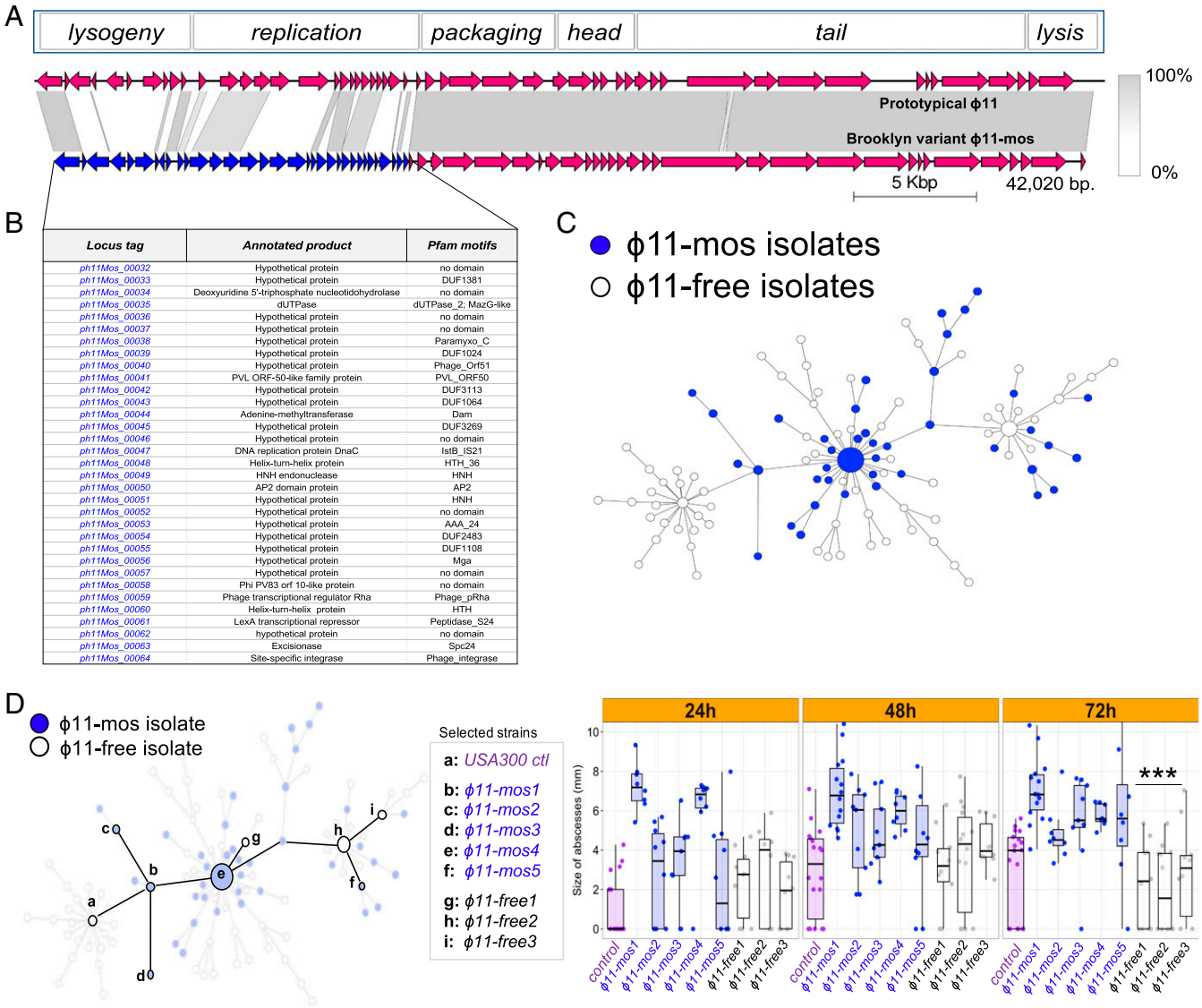

Locus tag	Annotated product	Pfam motifs
ph11Mos_00032	Hypothetical protein	no domain
ph11Mos_00033	Hypothetical protein	DUF1381
ph11Mos_00034	Deoxyuridine 5'-triphosphate nucleotidohydrolase	no domain
ph11Mos_00035	dUTPase	dUTPase_2; MazG-like
ph11Mos_00036	Hypothetical protein	no domain
ph11Mos_00037	Hypothetical protein	no domain
ph11Mos_00038	Hypothetical protein	Paramyxo_C
ph11Mos_00039	Hypothetical protein	DUF1024
ph11Mos_00040	Hypothetical protein	Phage_Orf51
ph11Mos_00041	PVL ORF-50-like family protein	PVL_ORF50
ph11Mos_00042	Hypothetical protein	DUF3113
ph11Mos_00043	Hypothetical protein	DUF1064
ph11Mos_00044	Adenine-methyltransferase	Dam
ph11Mos_00045	Hypothetical protein	DUF3269
ph11Mos_00046	Hypothetical protein	no domain
ph11Mos_00047	DNA replication protein DnaC	IstB_IS21
ph11Mos_00048	Helix-turn-helix protein	HTH_36
ph11Mos_00049	HNH endonuclease	HNH
ph11Mos_00050	AP2 domain protein	AP2
ph11Mos_00051	Hypothetical protein	HNH
ph11Mos_00052	Hypothetical protein	no domain
ph11Mos_00053	Hypothetical protein	AAA_24
ph11Mos_00054	Hypothetical protein	DUF2483
ph11Mos_00055	Hypothetical protein	DUF1108
ph11Mos_00056	Hypothetical protein	Mga
ph11Mos_00057	Hypothetical protein	no domain
ph11Mos_00058	Phi PV83 orf 10-like protein	no domain
ph11Mos_00059	Phage transcriptional regulator Rha	Phage_pRha
ph11Mos_00060	Helix-turn-helix protein	HTH
ph11Mos_00061	LexA transcriptional repressor	Peptidase_S24
ph11Mos_00062	hypothetical protein	no domain
ph11Mos_00063	Excisionase	Spc24
ph11Mos_00064	Site-specific integrase	Phage_integrase

Fig. 3. USA300-BKV isolates (BKV isolates) characterized by the presence of mosaic ϕ11 (ϕ11-mos) demonstrate enhanced virulence in a murine abscess model of infection compared with phage-free control USA300 isolates. (*A*) Comparative genome map of the prototypical ϕ11 and the BKV isolate-associated ϕ11-mos. Arrows indicate predicted ORFs and the direction of the transcription in phage functional modules. Unique ORFs are indicated in blue. (*B*) Genes encoding proteins with low homology between the BKV isolate-associated ϕ11-mos and prototypical ϕ11 are indicated. (*C*) Distribution of ϕ11-mos among BKV isolates (blue). (*D*) Selected BKV isolates ($n = 8$) from the minimum spanning tree representing a set of phage-free ($n = 3$) and ϕ11-mos–containing BKV isolates ($n = 5$). Size of murine skin lesions [($n = 10$) five mice per group with two abscesses per mouse] at 24, 48, and 72 h after s.c. infection with ~1×10^7 cfu of the indicated strain. Statistical analyses were performed with the Kruskal–Wallis test; ***$P < 0.001$. The results were corrected for multiple comparisons by using the Bonferroni-corrected threshold.

chromosome of USA300-LAC), and (*ii*) genes encoded within the mosaic portion of the phage enhance virulence. Additional studies are needed to determine to what extent mutation of *pyrR*, or other polymorphisms specific to the USA-BKV clone, modulate the effect of mosaic ϕ11. Notably, in vitro cytotoxicity failed to correlate with abscess size or phage content, suggesting that the changes that accompany phage-mediated enhanced virulence in the skin require host tissue-specific signals in vivo.

Identification of a *Staphylococcus* Epidermidis-Derived Mupirocin and Chlorhexidine Resistance Plasmid Driving Expansion of USA300-BKV Clones. DNA contigs derived from de novo DNA sequencing of all USA300-BKV strains were used to query publicly available databases [National Center for Biotechnology Information (NCBI)], resulting in identification of three plasmids. Two plasmids, present in all USA300-BKV isolates, closely matched plasmid pUSA01_ISMMS (CP007177.1), which encodes penicillinase (*blaZ*) and kanamycin resistance (*aphA*-3), and pUSA01 (NC_007790), a cryptic plasmid with no clear function. Both plasmids are widely distributed among USA300 clones (58–61).

The third plasmid, designated pBSRC1, did not demonstrate homology to any known sequence. To assemble pBSRC1 sequences, two USA300-BKV isolates (BKV_A1 and BKV_A2, Dataset S1) were selected for PacBio *RSII* long-read sequencing. Plasmid pBSRC1, obtained from USA300-BKV isolate BKV_A2, was ~38 kb long and contained 46 coding sequences (Fig. 5*A*) that included the *mupA* and *qacA/B* genes, which encode resistance to the widely used topical antimicrobials mupirocin and chlorhexidine, respectively. The pBSRC1 coding sequence matched a mixture of *S. aureus* and *Staphylococcus epidermidis* sequences (Fig. 5*A*).

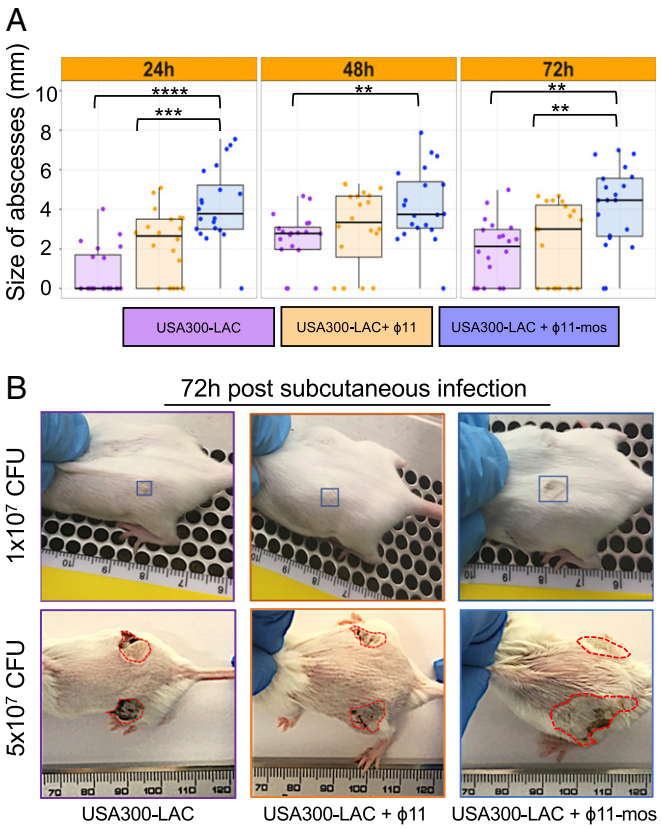

Fig. 4. The mosaic portion of ϕ11 increases skin abscess size. USA300-LAC lysogens of mosaic ϕ11 [(ϕ11-mos) produced by induction of USA300-BKV_28] and prototypical ϕ11 (produced by induction of RN451), which differ only in the region corresponding to the mosaic block, were made and compared in a murine abscess model of infection. (*A*) Abscess size at 24, 48, and 72 h after s.c. infection with ~1×10^7 cfu of the indicated strain [($n = 10$) five mice per group with two abscesses per mouse]. Statistical analyses were performed with the Kruskal–Wallis test after multiple comparison correction. (*B*) Representative pictures of murine skin abscesses at 3 d after s.c. infection with the indicated strain at either a 1×10^7 (*Top*) or a 5×10^7 cfu (*Bottom*) inoculum.

Transduction of pBSRC1 to recipient strain JE2, a laboratory USA300 strain (CP020619), resulted in high-level resistance to mupirocin [minimal inhibitory concentration (MIC) >1,024 μg/mL] (Dataset S1). High-level mupirocin resistance is frequent among USA300 clades that are associated with pediatric populations in New York City (62). Since no standardized method for testing susceptibility to chlorhexidine exists, resistance is usually defined by the presence of *qacA/B*, which increases the risk of persistent MRSA carriage after decolonization therapy (63–66). Broth dilution assays demonstrated a twofold MIC increase (from 2 to 4 μg/mL) for chlorhexidine in transductants (Dataset S1), consistent with *qacA/B*–associated resistance levels reported in previous studies of USA300 strains (67, 68).

We next examined the consequences of plasmid presence in the context of the dissemination of the USA300-BKV clone. We used a network analysis approach based on patristic distances to visualize genetic relationships between each USA300-BKV isolate. Although evolution of the clone began in a linear manner, a dominant variant emerged during dissemination of the USA300-BKV clone within the community (Fig. 5*B*, *Top*).

pBSRC1 was identified in most [88% (76/86)] USA300-BKV clones. *mupA* was always associated with pBSRC1, the presence of which correlated with the emergence of the dominant subclone (Fig. 5*B*, *Middle*). *qacA/B*-containing plasmids were found in 44 isolates (49%) and were always associated with the presence of *mupA* (Fig. 5*B*, *Bottom* and Dataset S1). To date the acquisition of *mupA* and *qac* genes, we performed an ancestral reconstruction using a time-scaled analysis based on the maximum parsimony tree (*SI Appendix*, Fig. S5). The results indicated that primary acquisition of *mupA* was, for the most part, followed by acquisition of *qacA/B*. Collectively, these data suggest that the USA300-BKV variants containing pBSRC1, a dual-resistance plasmid, arose during dissemination, became dominant, and accounted for the majority of isolates during the sampling period.

pBSRC1 sequences always included the 3.1-kb cryptic pUSA01 plasmid. Thus, the probable path of evolution of pBSRC1 was sequential recombination of a mosaic plasmid containing elements from *S. aureus* and *S. epidermidis* onto an indigenous cryptic plasmid (Fig. 5*C*).

Discussion

We report the spread of a unique USA300 clone of CA-MRSA that was limited exclusively to an Orthodox Jewish community in Brooklyn, suggesting a previously unrecognized high-risk population. Comprehensive genomic analysis and virulence assays identified a clone-specific prophage and a metabolic change that promoted abscess formation and colonization, respectively; they appear to have primed the clonal variant for success. Key events in clonal expansion were acquisitions of resistance genes to mupirocin and chlorhexidine, agents commonly used for decolonization and prevention of infection. These adaptations in virulence and resistance, when expanded from the high-risk community to the general human population, would constitute a serious public health threat.

As expected, the USA300-BKV clone carried a number of distinct nonsynonymous mutations that were present in all isolates. These mutations primarily affected genes involved in amino acid, carbohydrate, and nucleotide biosynthesis pathways, suggesting that metabolic adaptability was critical for success of the USA300-BKV clone. Our data indicate that differences in pyrimidine metabolic pathways in the USA300-BKV strain may be advantageous in high-risk populations, both because nucleotide metabolism is linked to the expression and synthesis of virulence factors (69) and because such differences provide a priming mechanism for growth in infectious ecologies where nutrients are scarce (70).

Genomic comparisons also showed that a unique phage, present in early USA300-BKV isolates, promotes large skin abscesses that may drive CA-MRSA contagion. More detailed analysis is required to define the mosaic phage components driving the enhanced skin virulence phenotype. Intriguingly, the mosaic portion of the prophage DNA that produced virulence encodes a methyltransferase/endonuclease restriction modification (RM) system (Fig. 4*B*). RM systems have been associated with increased virulence and clonal spread during an outbreak of Shiga toxin-producing *E. coli* O104:H4 (71, 72). Regardless of whether the methylase is found to be important in staphylococcal virulence, the absence of known virulence genes encoded within the phage supports a growing body of evidence that the regulation of bacterial genes, rather than the production of a virulence factor, confers increased fitness (73–75). Interestingly, the mosaic phage was associated with virulence phenotypes in vivo, but not in vitro, suggesting that an in vivo signal is required for phage-mediated up-regulation of virulence, and potentially explaining why the involvement of lysogeny in virulence has few precedents in *S. aureus* research. It is also worth noting that competence for DNA uptake in staphylococci depends on the presence of bacteriophage (76–78). Thus, sequential assimilation of plasmid DNA and chlorhexidine resistance elements may have been facilitated by the recombinant ϕ11 that was initially present within USA300-BKV isolates.

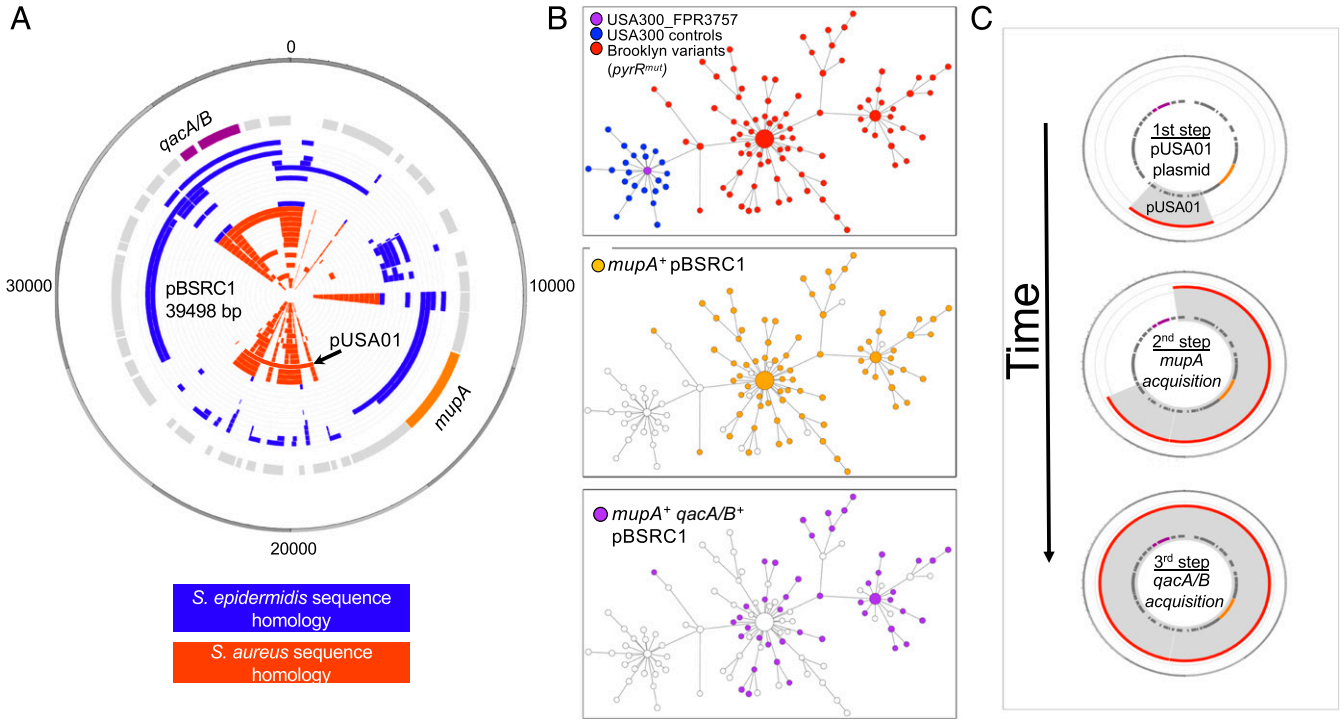

Fig. 5. Emergence of a dominant clone coincides with acquisition of an *S. epidermidis*-recombinant mupirocin resistance plasmid, pBSRC1. (*A*) Structure and characteristics of pBSRC1. Gene names and location are indicated in the first inner circle (gray). *mupA* and *qacA/B* are highlighted in orange and purple, respectively. Other inner circles show perfect BLAST homology results to *S. epidermidis* (blue) and *S. aureus* (red) plasmid sequences. The site of *S. aureus* pUSA01 integration in pBSRC1 is indicated. (*B*) Minimum spanning tree (MST) based on a patristic genetic comparison of 86 isolates obtained from patients residing in Orthodox-associated zip codes compared with 22 control USA300 isolates from adults and children in the same hospital (16 representative USA300 isolates from patients residing in non–high-risk zip codes, and six USA300 strains from Orthodox-associated zip-codes that were not part of the USA300-BKV clade). The first MST (*Top*) shows control strains (blue) and the USA300-BKV isolates (red). The second MST (*Middle*) highlights the distribution of *mupA*$^+$ pBSRC1 containing strains (orange), whereas the third MST (*Bottom*) represents the distribution of *qacA/B* pBSRC1 containing strains (purple). Each node represents a single strain. Distance between nodes is arbitrary, whereas node size is proportional to the number of connections. (*C*) Working model of the stepwise assembly of pBSRC1 in USA300-BKV isolates.

Selectively advantageous changes that spread through the bacterial population will fall on distal phylogenetic branches. Thus, our data indicating that evolution of the pBSRC1 plasmid containing dual-biocide resistance coincided with the emergence of successful variants strongly suggest that this plasmid and decolonization therapy were key events in clonal spread. The pBSRC1 plasmid originated from interspecies DNA exchange of *S. epidermidis* and *S. aureus* sequences plus recombination with an indigenous cryptic plasmid, pUSA01 (Fig. 3). These data suggest that cryptic plasmids can serve as an anchor for the stepwise acquisition of elements from both species. Acquisition of the arginine catabolic mobile element of *S. epidermidis* by USA300 is thought to have expanded its colonization niche to the skin, increasing opportunities for abscess formation and transmission (19). Collectively, these observations point to a potential reservoir of genes in otherwise nonpathogenic staphylococcal species that primarily confer a commensal fitness advantage rather than an enhanced capacity for infection.

In conclusion, high-resolution bacterial genomics and field surveillance of clinical strains provide insight into how heightened infection risk and clinical intervention remodel pathogens with respect to virulence and antimicrobial resistance. Broadly speaking, these data lead to a two-stage framework for interpreting the phenotypes of newly emergent clones. Early on, an introduction to a vulnerable population selects for genetic changes, such as *pyrR* mutation and phage acquisition, that drive bacterial emergence. These data highlight the need for vigorous surveillance and early public health intervention to limit further adaptation. In later stages, clinical intervention and control measures select for rapidly spreading determinants of success, such as plasmid-borne dual resistance to chlorhexidine and mupirocin. The temporal connection between these two processes links virulence and antimicrobial resistance, potentially explaining the convergence of *pvl*-mediated abscess formation and methicillin resistance in CA-MRSA lineages. The result is high-consequence clones and DNA elements that threaten larger human populations, including vulnerable populations in hospitals. Unique epidemiology and pathogens make the course of dissemination unpredictable, complicating efforts to plan for the next high-risk clone. Nonetheless, we expect that a better understanding of principles and infection traits involved in the epidemiology (e.g., virulence, metabolism, and resistance) will (*i*) uncover new vulnerabilities that can be exploited for prevention and treatment, and (*ii*) facilitate integration of genomic and epidemiological analysis, allowing more effective targeting of intervention strategies.

At a more global level, the present report demonstrates how the relationship between virulence and transmissibility (79) in pathogens such as CA-MRSA, in which disease and transmission are tightly linked, can lead to a new antimicrobial-resistance threat. Historically, antimicrobial-resistant clones of *S. aureus* disseminate globally. To interrupt this evolutionary pattern, our results suggest that the focus of preventative strategies targeting CA-MRSA should be to influence virulence so that the infective capacity is never attained.

Methods

Study Design and Facility. Children's services at New York University Langone Medical Center (NYCLMC) consist of 109 beds within a larger 1,069-bed tertiary care academic medical center. The general medicine ward, pediatric ward, and ICUs manage about 24,500, 1,700, and 600 admissions a year,

respectively. Ethical approval and informed consent were not required for the colonization study because all patients are routinely screened for *S. aureus* and MRSA nasal and throat carriage within 48 h of admission to the general pediatric ward and ICU as part of surveillance and management of health care-associated infection. Approval for medical record reviews, laboratory studies, and genome sequencing was granted by the NYULMC Institutional Review Board.

Bacterial isolates or genome sequences were obtained from three patient groups. The first group consisted of 84 consecutive single-patient isolates from pediatric patients residing in Orthodox-associated (high-risk) zip codes collected over a 2-y period from the clinical microbiology laboratory (cases, BKV_isolates, Dataset S1). Isolates were identified from every child 18 y old and younger having a high-risk zip code admitted to the general pediatric ward and ICU from May 2015 to May 2017. Eleven additional isolates were obtained from adults residing in high-risk zip codes who were admitted to the general medicine wards (BKV_A_isolates). Sites of infection and patient age are listed in Dataset S1. The second group consisted of 16 consecutive single-patient USA300 strains, including children admitted to the general pediatric ward and pediatric ICU (Ctl_isolates). Controls were collected from January 2016 to June 2016, after the clonality of isolates was established. Control zip codes represented each of the five New York City boroughs. Clonality was assigned by genotyping using a combination of methods, outlined below, as part of routine surveillance of MRSA by the NYULMC Molecular Outbreak Center. The third group consisted of 68 genome sequences of USA300 control isolates from single patients, collected and characterized in a large, community-based case-control study of CA-MRSA in northern Manhattan and the Bronx (24).

Bacterial Strains, Phage Sources, and Growth Conditions. Clinical isolates and laboratory strains USA300-LAC (AH-LAC) and USA300-JE2 (80, 81) were used in all experiments. For *pyrR* complementation, SapI1 integration vector pJC1111 was used to chromosomally integrate the WT *pyrR*, amplified using primers pyrR-F-PstI ATATCTGCAGGATACAATTCGAAAAAGAGA and pyrR-R-BamHI ATATGGATCCGTACTGAATTAAAAGGGGTA, incorporating the endogenous promoter into the SaPI1 attC site of RN9011, as described (82). Phage 80α was used to transduce the allele into JE2 or the indicated USA300-BVK strain (83); transductants were selected on tryptic soy agar (TSA) plates containing the appropriate antimicrobial (Cd). Phage 80α was also used to transduce plasmid pBSRC1 from USA300-BKV_02 into recipient strain AH-LAC. Prototype ϕ11 and mosaic ϕ11 were obtained by mitomycin C induction of RN451 (84), which is considered to be free of prophages except for ϕ11, and clinical isolate USA300-BKV_28, respectively. USA300-AH-LAC was lysogenized as described previously (83) by plaque-purified ϕ11 and mosaic ϕ11 to create strain AH-LAC + ϕ11 and AH-LAC + mosaic ϕ11, respectively. Cells were cultured in tryptic soy broth (TSB) (Difco) or Roswell Park Memorial Institute culture medium (RPMI) 1640 (Invitrogen) supplemented with 1% casamino acids or complete defined medium [CDM; Pattee/Neveln medium (85)] with constant aeration shaking (180 rpm) or on TSA plates. Incubation was at 37 °C. Growth curves were carried out in 200-μL cultures within a 96-well plate, which was inoculated using overnight cultures of three independent colonies for each strain and then washed three times in PBS and diluted 1:1,000 in fresh medium. Optical densities at 600 nm were read at the beginning of the subculture and at the indicated time points using a Bioscreen C Analyzer.

Mouse Model of Colonization and Transmission. We adaptated the infant mouse model to the study of CA-MRSA shedding and transmission. Intestinal carriage of *S. aureus* is frequent in human infants (86–88) and is thought to decrease toward adulthood. Unlike adult mice (89, 90), infant mice are highly susceptible hosts for which colonization and intralitter transmission of pathogens has been demonstrated without the use of antimicrobials (91–93). For competition experiments, WT reference strain LAC was grown separately from the *pyrR*-complemented strains overnight at 37 °C, diluted 100-fold, subcultured for 4 h, and mixed at a 1:1 ratio of 5×10^6 cfu. Pregnant C57BL/6J mice were obtained from The Jackson Laboratory and maintained in the Alexandria Center for Life Science West Tower animal facility. Seven-day-old pups were mouth-fed with 10^7 cfu of *S. aureus* suspended in 10 μL of sterile PBS with 20% sucrose using a blunt pipette tip. After the pup swallowed the inoculum, it was returned to its dam. In each cage, half of the pups were inoculated to study colonization, cohoused with the rest of the pups from which transmissions were detected. Cecal contents are used to evaluate colonization in infant mice, since they do not excrete stool pellets. Four days postinoculation, pups were killed by CO_2 asphyxiation followed by decapitation, and the cecum was collected and resuspended in 1 mL of sterile PBS followed by homogenization using a FastPrep-24 Classic Instrument (MP Biomedicals). The cecal suspension was then performed by 10-fold serial dilutions and plated on CHROMID MRSA SMART II agar (bioMérieux). The limit of detection was 10 cfu/mL. Colonies recovered from CHROMID MRSA SMART II agar were subsequently plated on TSB with 0.25 mM $CdCl_2$ to distinguish *pyrR*-complemented strains and WT. The amount of WT bacteria was calculated by subtracting the number of colonies that grew on $CdCl_2$-containing plates from the number of colonies formed on CHROMID MRSA SMART II plates.

Genotyping, Sequencing. All strains were genotyped by DNA sequence analysis of the protein A gene variable repeat region (*spa* typing) and a variety of additional DNA polymorphisms, including SCC*mec*, and the presence of the ACME and *pvl* genes as previously described (94, 95). USA300 lineage was defined by the presence of SCC*mec*IV, ACME, *pvl*, and assignment to clonal complex 8 by *spa* type using the Ridom SpaServer database (spa.ridom.de/mlst.shtml).

Genome Sequencing, Assembly, and Annotation. We prepared sequencing libraries from DNA extracted from each MRSA isolate as previously described (24, 96). Whole-genome sequencing was performed using Illumina HiSeq 2000 with 100-base paired-end reads or a PacBio *RSII* instrument (24, 49, 96). Paired-end Illumina reads were mapped against USA300_FPR3757 reference genome using Burrows-Wheeler Aligner (BWA) (97). BWA outputs were analyzed and annotated using SAMtools (97), GATK (98), and ANNOVAR (99). SNPs in genes annotated as integrases, transposases, resolvases, maturases, or phages were removed from the analysis using custom scripts. Other mobile genetic elements, including SaPI5, phiSA2usa, phiSA3usa, SCC*mec*IV, and ACME, were identified using IslandPath-DIMOB and PHASTSNPs (100, 101). Raw (PacBio) long-read data were assembled using the HGAP3 version 2.2.0 pipeline (102). Subsequently, a custom postassembly pipeline (https://github.com/powerpak/pathogendb-pipeline) was used to finalize each genome. Genes were annotated using Prokka (103), and genomes were visualized using ChomoZoom (104).

Raw Illumina reads from Harris et al. (33) were downloaded from the NCBI and mapped against *S. aureus* HO-5096-0412 reference genome (HE681097.1). SNPs were identified, and genes sharing mutations in all high-risk strains were compared with our list of mutated genes. De novo assemblies were performed on unmapped Illumina reads selected using BWA, and contigs were generated using Velvet with the Velvet Optimizer (105). Contigs larger than 100 bp (n = 276) were subjected to BLAST to identify large sequence polymorphisms.

Phylogenetic Analyses. Phylogenetic analysis was based on 5,326 high-confidence variable positions by specifying *S. aureus* MRSA131 (GCA_000187145.1) as the outgroup. Maximum-likelihood phylogenies with 1,000 bootstrap replications were obtained using PhyML (106) and the HKY model. These analyses included the two groups of control isolates from our hospital (n = 27) or the community-based case-control study in northern Manhattan (n = 68) (24). Evolutionary rates and time of emergence were determined using BEAST 1.7.5 package (107). BEAST was run for 100 million generations, sampling every 10,000 states using the HKY substitution model and strict, exponential-relaxed and lognormal-relaxed molecular clocks. Minimum spanning trees were generated using a patristic distance matrix and the Fruchterman–Reingold layout from the ape and igraph R packages (108). Tree topologies for ancestral reconstructions were generated in PhyML. Ancestral state reconstructions were performed using the phangorn R package (version 2.4.0) with the accelerated transformation function; all states and transformations were given equal weight.

Quantitative Reverse Transcriptase–PCR (qRT-PCR). Isolation of total RNA from *S. aureus* cultures grown for 6 h in CDM was carried out using an RNeasy extraction kit, following the manufacturer's instructions and the method previously described by Carroll et al. (109). qRT-PCR was performed using a one-step reaction with Reverse Transcriptase Mastermix (QuantiTect) and SYBR Green Master Mix (Qiagen) in a 7300 Real-Time PCR system (Applied Biosystems). Specific primer sets (*SI Appendix*, Table S3) were used to detect *pyrR* (this study) and *carA* and *pyrB* [Kriegeskorte et al. (69)] genes. All genes were normalized to the housekeeping gene (the 16S rRNA gene). Fold change for target genes from *pyrR*-complemented strains relative to the corresponding genes in WT strains was determined using the threshold cycle ($2-\Delta\Delta CT$) method of analysis. Melting curve analyses were employed to verify specific single-product amplification.

Cytotoxicity Assays. Leukopaks were obtained from deidentified donors from the New York Blood Center where written consents were obtained from all participants. Human polymorphonuclear neutrophils (hPMNs) were purified as described previously (56). Bacteriologically supernatants obtained from

early logarithmic-phase growth, were used for differentiating cytotoxic activity. Briefly, overnight cultures were diluted with fresh TSB, and the diluted culture was regrown for 6 h at 37 °C. Bacteria were pelleted, and filtered culture supernatants were serially diluted and added to 2×10^5 hPMNs per well for a final volume of 100 μL per well RPMI 1640 supplemented with 10% FBS. hPMNs were intoxicated with the culture supernatant from the indicated strain for 2 h at 37 °C and 5% CO_2. hPMN viability was determined using CellTiter 96 Aqueous One Solution (Promega). Cells were mixed with CellTiter and incubated at 37 °C and 5% CO_2 for 1.5 h. Cell viability was measured by absorbance at 492 nm using a PerkinElmer Envision 2103 Multilabel reader (PerkinElmer).

Animal Infections. For the skin infections, one representative strain from each group was cultivated for 3 h in TSB, washed in 1× PBS and normalized to 5×10^8 cfu. Five-week-old female ND4 Swiss Webster mice (Envigo, Inc.) were anesthetized intraperitoneally using 300 μL of avertin [2,2,2-tribromoethanol dissolved in tert-Amyl-alcohol and diluted to a final concentration of 2.5% (vol/vol) in sterile saline]. A total of 100 μL of bacteria, resulting in a 1×10^7 or a 5×10^7 cfu inoculum, as indicated, was injected s.c. into both hind flanks of shaved mice (56, 57). Subsequent lesions were measured using a digital caliper (Fisher Scientific) every 24 h, and the abscess diameter was determined. To assess bacterial burden, 8-mm punch (Integra Miltex) biopsy samples were obtained from mouse lesions at 9 d postinfection, and the tissues were homogenized, serially diluted, and enumerated on TSA (110).

Statistical Methods. Statistically significant differences between survival curves were determined by log rank (Mantel–Cox) test. The results were corrected for multiple comparisons by using the Bonferroni-corrected threshold. Sizes of murine skin abscesses were compared using the Kruskal–Wallis test with a P value <0.05. For the proteomic data, a two-sided Student's t test was performed, correcting for multiple testing by controlling for false discovery rate (FDR) at 5% (permutation-based FDR).

Data Availability. All genomic data are available at the NCBI BioProject database under accession no. PRJNA497094. All other relevant data are within the paper and in Datasets S1 and S2 and *SI Appendix*.

ACKNOWLEDGMENTS. This study was supported by NIH Grant R01 AI103268 and NIH National Institute of Allergy and Infectious Diseases Grant HHSN272201400019C (to R.C., V.J.T., and B.S.); NIH Research Training Grant T32 AI007180 (to W.E.S.); NIH Grants R01 AI099394 and R01 AI105129 (to V.J.T.); KiDS of NYU (J.C.F.); a generous donation by Judith and Irwin Kallman (J.C.F.); NIH Grant R01 AI119145 (to H.v.B.); NIH Grant T32 AI07647; Clinical and Translational Science Awards Program at the National Center for Advancing Translational Sciences (CTSA/NCATS) Grant KL2TR001435; the New York State Department of Health Empire Clinical Research Investigator Program (D.R.A.); and NIH Grant 1K08AI101005 (to P.J.P.). V.J.T. is a Burroughs Wellcome Fund Investigator in the Pathogenesis of Infectious Diseases.

1. Ammerlaan HS, et al. (2013) Secular trends in nosocomial bloodstream infections: Antibiotic-resistant bacteria increase the total burden of infection. *Clin Infect Dis* 56: 798–805.
2. Moran GJ, et al.; EMERGEncy ID Net Study Group (2006) Methicillin-resistant *S. aureus* infections among patients in the emergency department. *N Engl J Med* 355: 666–674.
3. Popovich KJ, Weinstein RA, Hota B (2008) Are community-associated methicillin-resistant *Staphylococcus aureus* (MRSA) strains replacing traditional nosocomial MRSA strains? *Clin Infect Dis* 46:787–794.
4. Seybold U, et al. (2006) Emergence of community-associated methicillin-resistant *Staphylococcus aureus* USA300 genotype as a major cause of health care-associated blood stream infections. *Clin Infect Dis* 42:647–656.
5. David MZ, Daum RS (2010) Community-associated methicillin-resistant *Staphylococcus aureus*: Epidemiology and clinical consequences of an emerging epidemic. *Clin Microbiol Rev* 23:616–687.
6. Carlson JM, et al. (2014) HIV transmission. Selection bias at the heterosexual HIV-1 transmission bottleneck. *Science* 345:1254031.
7. Crawford H, et al. (2009) Evolution of HLA-B*5703 HIV-1 escape mutations in HLA-B*5703-positive individuals and their transmission recipients. *J Exp Med* 206:909–921.
8. Diehl WE, et al. (2016) Ebola virus glycoprotein with increased infectivity dominated the 2013-2016 epidemic. *Cell* 167:1088–1098.e6.
9. Pepin KM, Lass S, Pulliam JR, Read AF, Lloyd-Smith JO (2010) Identifying genetic markers of adaptation for surveillance of viral host jumps. *Nat Rev Microbiol* 8:802–813.
10. Pettersson JH, et al. (2016) How did Zika virus emerge in the Pacific Islands and Latin America? *MBio* 7:e01239-16.
11. Poon LL, et al. (2016) Quantifying influenza virus diversity and transmission in humans. *Nat Genet* 48:195–200.
12. Urbanowicz RA, et al. (2016) Human adaptation of ebola virus during the West African outbreak. *Cell* 167:1079–1087.e5.
13. DeLeo FR, et al. (2011) Molecular differentiation of historic phage-type 80/81 and contemporary epidemic *Staphylococcus aureus*. *Proc Natl Acad Sci USA* 108:18091–18096.
14. Harris SR, et al. (2010) Evolution of MRSA during hospital transmission and intercontinental spread. *Science* 327:469–474.
15. Kennedy AD, et al. (2008) Epidemic community-associated methicillin-resistant *Staphylococcus aureus*: Recent clonal expansion and diversification. *Proc Natl Acad Sci USA* 105:1327–1332.
16. Planet PJ, et al. (2017) Architecture of a species: Phylogenomics of *Staphylococcus aureus*. *Trends Microbiol* 25:153–166.
17. Young BC, et al. (2012) Evolutionary dynamics of *Staphylococcus aureus* during progression from carriage to disease. *Proc Natl Acad Sci USA* 109:4550–4555.
18. Fitzgerald JR, Holden MT (2016) Genomics of natural populations of *Staphylococcus aureus*. *Annu Rev Microbiol* 70:459–478.
19. Diep BA, et al. (2006) Complete genome sequence of USA300, an epidemic clone of community-acquired meticillin-resistant *Staphylococcus aureus*. *Lancet* 367:731–739.
20. Gallagher P (2009) Identification and analysis of Orthodox Jewish enclaves in Brooklyn, New York: A GIS based approach. *Middle States Geogr* 42:83–89.
21. David MZ, et al. (2013) Comparing pulsed-field gel electrophoresis with multilocus sequence typing, spa typing, staphylococcal cassette chromosome mec (SCC*mec*) typing, and PCR for panton-valentine leukocidin, *arcA*, and *opp3* in methicillin-resistant *Staphylococcus aureus* isolates at a U.S. Medical Center. *J Clin Microbiol* 51:814–819.
22. Strauß L, et al. (2017) Origin, evolution, and global transmission of community-acquired *Staphylococcus aureus* ST8. *Proc Natl Acad Sci USA* 114:E10596–E10604.
23. Hafer C, Lin Y, Kornblum J, Lowy FD, Uhlemann AC (2012) Contribution of selected gene mutations to resistance in clinical isolates of vancomycin-intermediate *Staphylococcus aureus*. *Antimicrob Agents Chemother* 56:5845–5851.
24. Benson MA, et al. (2014) Evolution of hypervirulence by a MRSA clone through acquisition of a transposable element. *Mol Microbiol* 93:664–681.
25. Tobisch S, Stülke J, Hecker M (1999) Regulation of the *lic* operon of *Bacillus subtilis* and characterization of potential phosphorylation sites of the LicR regulator protein by site-directed mutagenesis. *J Bacteriol* 181:4995–5003.
26. Nuxoll AS, et al. (2012) CcpA regulates arginine biosynthesis in *Staphylococcus aureus* through repression of proline catabolism. *PLoS Pathog* 8:e1003033.
27. Tojo S, Satomura T, Matsuoka H, Hirooka K, Fujita Y (2011) Catabolite repression of the *Bacillus subtilis* FadR regulon, which is involved in fatty acid catabolism. *J Bacteriol* 193:2388–2395.
28. Yamamoto H, Serizawa M, Thompson J, Sekiguchi J (2001) Regulation of the *glv* operon in *Bacillus subtilis*: YfiA (GlvR) is a positive regulator of the operon that is repressed through CcpA and cre. *J Bacteriol* 183:5110–5121.
29. Stülke J, Hillen W (1999) Carbon catabolite repression in bacteria. *Curr Opin Microbiol* 2:195–201.
30. Turnbough CL, Jr, Switzer RL (2008) Regulation of pyrimidine biosynthetic gene expression in bacteria: Repression without repressors. *Microbiol Mol Biol Rev* 72: 266–300.
31. Ghim SY, Switzer RL (1996) Mutations in *Bacillus subtilis* PyrR, the *pyr* regulatory protein, with defects in regulation by pyrimidines. *FEMS Microbiol Lett* 137:13–18.
32. Savacool HK, Switzer RL (2002) Characterization of the interaction of *Bacillus subtilis* PyrR with *pyr* mRNA by site-directed mutagenesis of the protein. *J Bacteriol* 184: 2521–2528.
33. Harris SR, et al. (2013) Whole-genome sequencing for analysis of an outbreak of meticillin-resistant *Staphylococcus aureus*: A descriptive study. *Lancet Infect Dis* 13: 130–136.
34. Date SV, et al. (2014) Global gene expression of methicillin-resistant *Staphylococcus aureus* USA300 during human and mouse infection. *J Infect Dis* 209:1542–1550.
35. Szafranska AK, et al. (2014) High-resolution transcriptomic analysis of the adaptive response of *Staphylococcus aureus* during acute and chronic phases of osteomyelitis. *MBio* 5:e01775-14.
36. Valentino MD, et al. (2014) Genes contributing to *Staphylococcus aureus* fitness in abscess- and infection-related ecologies. *MBio* 5:e01729-14.
37. Wilde AD, et al. (2015) Bacterial hypoxic responses revealed as critical determinants of the host-pathogen outcome by TnSeq analysis of *Staphylococcus aureus* invasive infection. *PLoS Pathog* 11:e1005341.
38. Faden H, et al. (2010) Importance of colonization site in the current epidemic of staphylococcal skin abscesses. *Pediatrics* 125:e618–e624.
39. McCullough AC, et al. (2011) Higher incidence of perineal community acquired MRSA infections among toddlers. *BMC Pediatr* 11:96.
40. Gagnaire J, et al. (2017) Epidemiology and clinical relevance of *Staphylococcus aureus* intestinal carriage: A systematic review and meta-analysis. *Expert Rev Anti Infect Ther* 15:767–785.
41. Kumar N, David MZ, Boyle-Vavra S, Sieth J, Daum RS (2015) High *Staphylococcus aureus* colonization prevalence among patients with skin and soft tissue infections and controls in an urban emergency department. *J Clin Microbiol* 53:810–815.
42. Piewngam P, et al. (2018) Pathogen elimination by probiotic *Bacillus* via signalling interference. *Nature* 562:532–537.
43. Vogel-Scheel J, Alpert C, Engst W, Loh G, Blaut M (2010) Requirement of purine and pyrimidine synthesis for colonization of the mouse intestine by *Escherichia coli*. *Appl Environ Microbiol* 76:5181–5187.
44. Yang HJ, Bogomolnaya L, McClelland M, Andrews-Polymenis H (2017) *De novo* pyrimidine synthesis is necessary for intestinal colonization of *Salmonella Typhimurium* in chicks. *PLoS One* 12:e0183751.

45. Iandolo JJ, et al. (2002) Comparative analysis of the genomes of the temperate bacteriophages phi 11, phi 12 and phi 13 of *Staphylococcus aureus* 8325. *Gene* 289: 109–118.
46. Xia G, Wolz C (2014) Phages of *Staphylococcus aureus* and their impact on host evolution. *Infect Genet Evol* 21:593–601.
47. Maiques E, et al. (2006) beta-lactam antibiotics induce the SOS response and horizontal transfer of virulence factors in *Staphylococcus aureus*. *J Bacteriol* 188: 2726–2729.
48. Ubeda C, et al. (2005) Antibiotic-induced SOS response promotes horizontal dissemination of pathogenicity island-encoded virulence factors in staphylococci. *Mol Microbiol* 56:836–844.
49. Altman DR, et al. (2018) Genome plasticity of *agr*-defective Staphylococcus aureus during clinical infection. *Infect Immun* 86:e00331-18.
50. Goerke C, et al. (2004) Increased frequency of genomic alterations in *Staphylococcus aureus* during chronic infection is in part due to phage mobilization. *J Infect Dis* 189: 724–734.
51. Goerke C, Wirtz C, Flückiger U, Wolz C (2006) Extensive phage dynamics in *Staphylococcus aureus* contributes to adaptation to the human host during infection. *Mol Microbiol* 61:1673–1685.
52. Salgado-Pabón W, et al. (2014) Staphylococcus aureus β-toxin production is common in strains with the β-toxin gene inactivated by bacteriophage. *J Infect Dis* 210: 784–792.
53. Sampedro GR, et al. (2014) Targeting Staphylococcus aureus α-toxin as a novel approach to reduce severity of recurrent skin and soft-tissue infections. *J Infect Dis* 210: 1012–1018.
54. Wang R, et al. (2007) Identification of novel cytolytic peptides as key virulence determinants for community-associated MRSA. *Nat Med* 13:1510–1514.
55. Li M, et al. (2010) Comparative analysis of virulence and toxin expression of global community-associated methicillin-resistant *Staphylococcus aureus* strains. *J Infect Dis* 202:1866–1876.
56. Balasubramanian D, et al. (2016) *Staphylococcus aureus* coordinates leukocidin expression and pathogenesis by sensing metabolic fluxes via RpiRc. *MBio* 7:e00818-16.
57. Cho JS, et al. (2010) IL-17 is essential for host defense against cutaneous *Staphylococcus aureus* infection in mice. *J Clin Invest* 120:1762–1773.
58. Glaser P, et al. (2016) Demography and intercontinental spread of the USA300 community-acquired methicillin-resistant *Staphylococcus aureus* lineage. *MBio* 7:e02183-15.
59. Kennedy AD, et al. (2010) Complete nucleotide sequence analysis of plasmids in strains of *Staphylococcus aureus* clone USA300 reveals a high level of identity among isolates with closely related core genome sequences. *J Clin Microbiol* 48:4504–4511.
60. Sabat AJ, et al. (2017) Complete-genome sequencing elucidates outbreak dynamics of CA-MRSA USA300 (ST8-*spa* t008) in an academic hospital of Paramaribo, Republic of Suriname. *Sci Rep* 7:41050.
61. Uhlemann AC, et al. (2014) Molecular tracing of the emergence, diversification, and transmission of *S. aureus* sequence type 8 in a New York community. *Proc Natl Acad Sci USA* 111:6738–6743.
62. Antonov NK, et al. (2015) High prevalence of mupirocin resistance in *Staphylococcus aureus* isolates from a pediatric population. *Antimicrob Agents Chemother* 59: 3350–3356.
63. Batra R, et al. (2010) Efficacy and limitation of a chlorhexidine-based decolonization strategy in preventing transmission of methicillin-resistant *Staphylococcus aureus* in an intensive care unit. *Clin Infect Dis* 50:210–217.
64. Johnson RC, et al. (2015) Recurrent methicillin-resistant *Staphylococcus aureus* cutaneous abscesses and selection of reduced chlorhexidine susceptibility during chlorhexidine use. *J Clin Microbiol* 53:3677–3682.
65. Lee AS, et al. (2011) Impact of combined low-level mupirocin and genotypic chlorhexidine resistance on persistent methicillin-resistant *Staphylococcus aureus* carriage after decolonization therapy: A case-control study. *Clin Infect Dis* 52: 1422–1430.
66. Wassenaar TM, Ussery D, Nielsen LN, Ingmer H (2015) Review and phylogenetic analysis of *qac* genes that reduce susceptibility to quaternary ammonium compounds in *Staphylococcus* species. *Eur J Microbiol Immunol (Bp)* 5:44–61.
67. Mc Gann P, et al. (2013) Rapid and simultaneous detection of the chlorhexidine and mupirocin resistance genes *qacA/B* and *mupA* in clinical isolates of methicillin-resistant *Staphylococcus aureus*. *Diagn Microbiol Infect Dis* 77:270–272.
68. Schlett CD, et al. (2014) Prevalence of chlorhexidine-resistant methicillin-resistant *Staphylococcus aureus* following prolonged exposure. *Antimicrob Agents Chemother* 58:4404–4410.
69. Kriegeskorte A, et al. (2014) Inactivation of *thyA* in *Staphylococcus aureus* attenuates virulence and has a strong impact on metabolism and virulence gene expression. *MBio* 5:e01447-14.
70. Samant S, et al. (2008) Nucleotide biosynthesis is critical for growth of bacteria in human blood. *PLoS Pathog* 4:e37.
71. Fang G, et al. (2012) Genome-wide mapping of methylated adenine residues in pathogenic *Escherichia coli* using single-molecule real-time sequencing. *Nat Biotechnol* 30:1232–1239.
72. Forde BM, et al. (2015) Lineage-specific methyltransferases define the methylome of the globally disseminated *Escherichia coli* ST131 clone. *MBio* 6:e0160215.
73. Chen Y, Golding I, Sawai S, Guo L, Cox EC (2005) Population fitness and the regulation of *Escherichia coli* genes by bacterial viruses. *PLoS Biol* 3:e229.
74. Tree JJ, Granneman S, McAteer SP, Tollervey D, Gally DL (2014) Identification of bacteriophage-encoded anti-sRNAs in pathogenic *Escherichia coli*. *Mol Cell* 55: 199–213.
75. Wagner PL, Waldor MK (2002) Bacteriophage control of bacterial virulence. *Infect Immun* 70:3985–3993.
76. Rudkin JK, et al. (2012) Methicillin resistance reduces the virulence of healthcare-associated methicillin-resistant *Staphylococcus aureus* by interfering with the agr quorum sensing system. *J Infect Dis* 205:798–806.
77. Thompson NE, Pattee PA (1977) Transformation in *Staphylococcus aureus*: Role of bacteriophage and incidence of competence among strains. *J Bacteriol* 129:778–788.
78. Thompson NE, Pattee PA (1981) Genetic transformation in *Staphylococcus aureus*: Demonstration of a competence-conferring factor of bacteriophage origin in bacteriophage 80 alpha lysates. *J Bacteriol* 148:294–300.
79. Lipsitch M, Moxon ER (1997) Virulence and transmissibility of pathogens: What is the relationship? *Trends Microbiol* 5:31–37.
80. Boles BR, Thoendel M, Roth AJ, Horswill AR (2010) Identification of genes involved in polysaccharide-independent *Staphylococcus aureus* biofilm formation. *PLoS One* 5: e10146.
81. Fey PD, et al. (2013) A genetic resource for rapid and comprehensive phenotype screening of nonessential *Staphylococcus aureus* genes. *MBio* 4:e00537-12.
82. Chen J, Yoong P, Ram G, Torres VJ, Novick RP (2014) Single-copy vectors for integration at the SaPI1 attachment site for *Staphylococcus aureus*. *Plasmid* 76:1–7.
83. Novick RP (1991) Genetic systems in staphylococci. *Methods Enzymol* 204:587–636.
84. Novick R (1967) Properties of a cryptic high-frequency transducing phage in *Staphylococcus aureus*. *Virology* 33:155–166.
85. Richardson AR, Dunman PM, Fang FC (2006) The nitrosative stress response of *Staphylococcus aureus* is required for resistance to innate immunity. *Mol Microbiol* 61:927–939.
86. Björkstén B, Sepp E, Julge K, Voor T, Mikelsaar M (2001) Allergy development and the intestinal microflora during the first year of life. *J Allergy Clin Immunol* 108: 516–520.
87. Lindberg E, et al. (2004) High rate of transfer of *Staphylococcus aureus* from parental skin to infant gut flora. *J Clin Microbiol* 42:530–534.
88. Lindberg E, Nowrouzian F, Adlerberth I, Wold AE (2000) Long-time persistence of superantigen-producing *Staphylococcus aureus* strains in the intestinal microflora of healthy infants. *Pediatr Res* 48:741–747.
89. Kernbauer E, Maurer K, Torres VJ, Shopsin B, Cadwell K (2015) Gastrointestinal dissemination and transmission of *Staphylococcus aureus* following bacteremia. *Infect Immun* 83:372–378.
90. Misawa Y, et al. (2015) *Staphylococcus aureus* colonization of the mouse gastrointestinal tract is modulated by wall teichoic acid, capsule, and surface proteins. *PLoS Pathog* 11:e1005061.
91. Fernandez MI, et al. (2003) A newborn mouse model for the study of intestinal pathogenesis of shigellosis. *Cell Microbiol* 5:481–491.
92. Klose KE (2000) The suckling mouse model of cholera. *Trends Microbiol* 8:189–191.
93. Zafar MA, Kono M, Wang Y, Zangari T, Weiser JN (2016) Infant mouse model for the study of shedding and transmission during *Streptococcus pneumoniae* monoinfection. *Infect Immun* 84:2714–2722.
94. Diep BA, et al. (2008) The arginine catabolic mobile element and staphylococcal chromosomal cassette *mec* linkage: Convergence of virulence and resistance in the USA300 clone of methicillin-resistant *Staphylococcus aureus*. *J Infect Dis* 197: 1523–1530.
95. Mendes RE, et al. (2012) Characterization of methicillin-resistant *Staphylococcus aureus* strains recovered from a phase IV clinical trial for linezolid versus vancomycin for treatment of nosocomial pneumonia. *J Clin Microbiol* 50:3694–3702.
96. Altman DR, et al. (2014) Transmission of methicillin-resistant *Staphylococcus aureus* via deceased donor liver transplantation confirmed by whole genome sequencing. *Am J Transplant* 14:2640–2644.
97. Arias CA, Murray BE (2009) Antibiotic-resistant bugs in the 21st century–A clinical super-challenge. *N Engl J Med* 360:439–443.
98. McKenna A, et al. (2010) The Genome Analysis Toolkit: A MapReduce framework for analyzing next-generation DNA sequencing data. *Genome Res* 20:1297–1303.
99. Gardete S, et al. (2012) Genetic pathway in acquisition and loss of vancomycin resistance in a methicillin resistant *Staphylococcus aureus* (MRSA) strain of clonal type USA300. *PLoS Pathog* 8:e1002505.
100. Langille MG, Hsiao WW, Brinkman FS (2008) Evaluation of genomic island predictors using a comparative genomics approach. *BMC Bioinformatics* 9:329.
101. Zhou Y, Liang Y, Lynch KH, Dennis JJ, Wishart DS (2011) PHAST: A fast phage search tool. *Nucleic Acids Res* 39:W347–W352.
102. Chin CS, et al. (2013) Nonhybrid, finished microbial genome assemblies from long-read SMRT sequencing data. *Nat Methods* 10:563–569.
103. Seemann T (2014) Prokka: Rapid prokaryotic genome annotation. *Bioinformatics* 30: 2068–2069.
104. Pak TR, Roth FP (2013) ChromoZoom: A flexible, fluid, web-based genome browser. *Bioinformatics* 29:384–386.
105. Zerbino DR, Birney E (2008) Velvet: Algorithms for de novo short read assembly using de Bruijn graphs. *Genome Res* 18:821–829.
106. Guindon S, et al. (2010) New algorithms and methods to estimate maximum-likelihood phylogenies: Assessing the performance of PhyML 3.0. *Syst Biol* 59: 307–321.
107. Drummond AJ, Suchard MA, Xie D, Rambaut A (2012) Bayesian phylogenetics with BEAUti and the BEAST 1.7. *Mol Biol Evol* 29:1969–1973.
108. Csardi G, Nepusz T (2006) The igraph software package for complex network research. *Inter J Complex Syst* 1695:1–9.
109. Carroll RK, Weiss A, Shaw LN (2016) RNA-sequencing of *Staphylococcus aureus* messenger RNA. *Methods Mol Biol* 1373:131–141.
110. Leech JM, Lacey KA, Mulcahy ME, Medina E, McLoughlin RM (2017) IL-10 plays opposing roles during *Staphylococcus aureus* systemic and localized infections. *J Immunol* 198:2352–2365.